Modeling of the SLIPI technique with the large scatterer approximation of the RTE

Kristensson, Elias; Kristensson, Gerhard

Published in:
2017 32nd General Assembly and Scientific Symposium of the International Union of Radio Science

DOI:
10.23919/URSIGASS.2017.8105101

2017

Document Version:
Peer reviewed version (aka post-print)

32nd URSI GASS, Montreal, 19–26 August 2017

Modeling of the SLIPI technique with the large scatterer approximation of the RTE

Elias Kristensson(1) and Gerhard Kristensson*(2)
(1) Department of Physics, Division of Combustion Physics, Lund University, P.O. Box 118, SE-221 00 Lund, Sweden.
(2) Department of Electrical and Information Technology, Lund University, P.O. Box 118, SE-221 00 Lund, Sweden.

Abstract

To overcome the blur when visualizing of the interior of a turbid media by means light-based methods, a technique called Structured Laser Illumination Planar Imaging (SLIPI) is employed. The method is based on a 'light coding' strategy to distinguish between directly and multiply scattered light, allowing the intensity from the latter to be suppressed by post-processing data. In this paper, we explain the origin of the deviations between SLIPI measurements and the results obtained by the Bouguer-Beer law. The explanation employs the large scatterer approximation of the Radiative Transfer Equation. Our results indicate that forward-scattering can lead to deviations between experiments and theoretical predictions, especially when probing relatively large particles.

1 Introduction

Structured Laser Illumination Planar Imaging (SLIPI) is an optical imaging technique primarily used to visualize spray-related phenomena, such as the disintegration of liquid into fine, spherical droplets [1]. SLIPI is based on laser sheet imaging and structured illumination [2], which employs an intensity modulation scheme to permit sequential post-processing possibilities. When laser sheet technique is applied to highly scattering environments, multiple scattering effects dominate, which implies incorrect intensity levels compare to the results predicted by Bouguer-Beer law [1]. In particular, an increased particle size results in larger deviations from theoretical predictions. Electrically large particles have a pronounced forward scattering lobe, and since light that propagates in this direction preserves the line structure employed in SLIPI, it cannot be suppressed with the technique, thus resulting in the observed deviations from the Bouguer-Beer law. Light that has been scattered several times lose this structural information due to random averaging. By post-processing the acquired data, the latter unwanted contribution can be greatly suppressed, leading to improved visualization of turbid, scattering objects. An example of the process is given in Figure 1.

2 Experimental arrangements

A schematic of the experimental setup is presented in Figure 2 with a camera positioned at 90°, that records the signal that is generated by the laser sheet. Laser light of vacuum wavelength $\lambda = 447$ nm was used and a complete description of the experimental setup and sample preparation are found in [3].

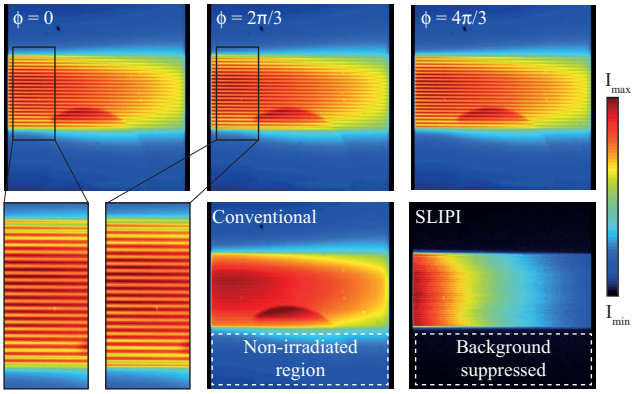

Figure 1: The SLIPI process illustrated on one of the cuvettes used in the current study.

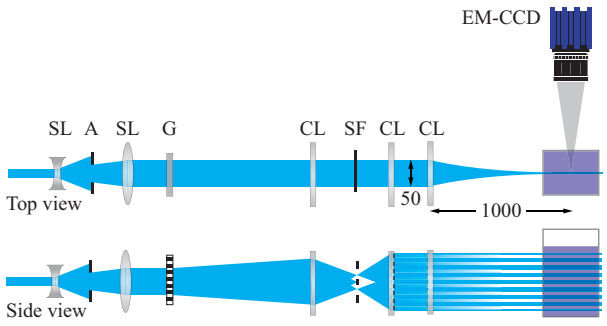

Figure 2: The experimental setup. SL = Spherical Lens. A = Aperture. G = Grating. CL = Cylinder Lens. SF = Spatial Filter.

Six suspensions of water and non-absorbing microspheres were used in the experiments with approximate diameters of 4.5, 6, 10, 15, 20 and 25 μm, respectively. These particles were assumed to be spherical. All mixtures were prepared to have an optical depth of $OD = 2$, where optical depth is defined as the sample length (44 mm) multiplied by the average extinction coefficient (number density times the extinction cross section σ_{ext}), in this case corresponding to a value of 0.045 mm^{-1}. When visualizing the scattered light from a spatially homogeneous sample of identical particle size, even minute changes in the collection- and accep-

tance angle affect the resulting image because of the rapid angular variations in the scattering phase function. This requires exact knowledge of the angle between laser sheet and the detector as well as the acceptance angles, which are both difficult to assess with sufficiently high precision. To circumvent the issue with the side-scattering lobes experimentally, a small amount of fluorescing dye was added to each mixture. Since the inelastic fluorescence signal (LIF) is nearly isotopic and identical for all mixtures under study, the exact position of the camera with respect to the laser sheet is no longer a critical factor. By compensating for the loss of light introduced by the added dye ($OD \approx 0.1$), the approach thus allowed monitoring of the relative loss of light intensity as a function of distance, without being influenced by the specifics of the detection system.

3 Theory

The 3D radiative transfer equation (RTE) [4] is commonly adopted as a model for computations of the intensity variations in random media. The RTE quantifies the intensity $I(\boldsymbol{r},\hat{\boldsymbol{n}})$ at a point $\boldsymbol{r}$ in the medium in a specific direction $\hat{\boldsymbol{n}}$. A vector formulation of RTE is available, but the experimental results in this paper have very little polarization information, and a scalar version of RTE suffices. In this paper, $ka \approx [30, 165]$, where k is the wave number of the microspheres relative to the background material in the cuvette (refractive index of $m = 1.60$ at $\lambda = 447$ nm [5]), and a is the radius of the spheres.

There are two main assumptions made in this paper, which dramatically simplify the solution of the RTE: (1) the homogeneity assumption, *i.e.*, σ_{ext} does not depend on location or incident directions, and (2) the forward scattering assumption, which is explained below. The pertinent scalar version of the radiative transfer equation (RTE) for a homogeneous suspension of spherical particles is, see *e.g.*, [4] (all distances are measured in units of the optical distance, OD, *i.e.*, $\boldsymbol{r}_{\text{OD}} = \boldsymbol{r} n_0 \sigma_{\text{ext}}$)

$$\hat{\boldsymbol{n}} \cdot \nabla_{\text{OD}} I(\boldsymbol{r}_{\text{OD}}, \hat{\boldsymbol{n}}) = -I(\boldsymbol{r}_{\text{OD}}, \hat{\boldsymbol{n}}) + \iint_{\Omega} p(\hat{\boldsymbol{n}} - \hat{\boldsymbol{n}}') I(\boldsymbol{r}_{\text{OD}}, \hat{\boldsymbol{n}}') \, \mathrm{d}\Omega' \quad (3.1)$$

where Ω denotes the unit sphere, n_0 the number density (number of scatterers per unit volume), σ_{ext} the extinction cross section, and where $p(\hat{\boldsymbol{n}} - \hat{\boldsymbol{n}}')$ denotes the phase function in the direction $\hat{\boldsymbol{n}}$ (incident direction $\hat{\boldsymbol{n}}'$).

4 Large scatterer approximation

The slab geometry of interest in this paper is depicted in Figure 3. The spheres are suspended in water between $0 \le z \le d$ or in terms of the scaled variables, $\tau = n_0 \sigma_{\text{ext}} z$, between $0 \le \tau \le \tau_0 = n_0 \sigma_{\text{ext}} d$. The scaled lateral variables are denoted $\boldsymbol{\eta} = n_0 \sigma_{\text{ext}} (x\hat{\boldsymbol{x}} + y\hat{\boldsymbol{y}})$. The final goal is to compute the light intensity in a neighborhood of the forward direction $\hat{\boldsymbol{n}} = \hat{\boldsymbol{z}}$. The direction $\hat{\boldsymbol{n}} = s_x\hat{\boldsymbol{x}} + s_y\hat{\boldsymbol{y}} + s_z\hat{\boldsymbol{z}}$, expressed in Cartesian coordinates, is subject to the constraint $s_x^2 + s_y^2 + s_z^2 = 1$. Most of the variation in the intensity takes place in the forward direction $s_z \approx 1$, *i.e.*, the scattering angle is small. Therefore, the directional derivative is approximated with

$$\hat{\boldsymbol{n}} \cdot \nabla_{\text{OD}} = s_z \frac{\partial}{\partial \tau} + \boldsymbol{s} \cdot \nabla_{\text{OD}} \approx \frac{\partial}{\partial \tau} + \boldsymbol{s} \cdot \nabla_{\text{OD}}$$

In the integral over the unit sphere, the lateral variable $\boldsymbol{s} = s_x\hat{\boldsymbol{x}} + s_y\hat{\boldsymbol{y}}$ is restricted by $s_x^2 + s_y^2 \le 1$, but due to the vanishing contribution of the phase function when $s_x^2 + s_y^2 > 1$, the integration in $\boldsymbol{s}$ can be extended to the entire x-y plane, without a major change in the value of the integral.

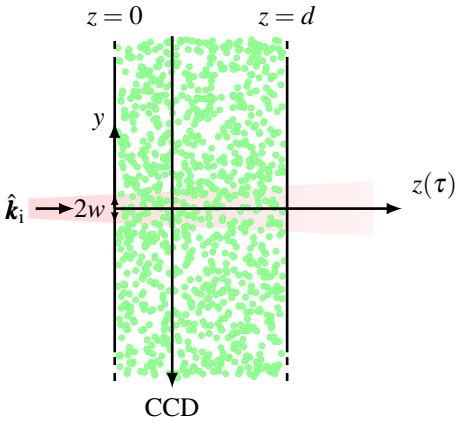

Figure 3: The geometry of a slab, seen from above, illuminated with a beam (laser sheet) of limited extent.

As a consequence of the assumptions made above, the RTE in (3.1) is approximated by

$$\frac{\partial}{\partial \tau} I(\boldsymbol{\eta}, \tau, \boldsymbol{s}) + \boldsymbol{s} \cdot \nabla_{\text{OD}} I(\boldsymbol{\eta}, \tau, \boldsymbol{s}) = -I(\boldsymbol{\eta}, \tau, \boldsymbol{s}) + \iint_{\mathbb{R}^2} p(\boldsymbol{s} - \boldsymbol{s}') I(\boldsymbol{\eta}, \tau, \boldsymbol{s}') \, \mathrm{d}\boldsymbol{s}'$$

It is assumed that the phase function has its main contribution for small arguments $|\boldsymbol{s} - \boldsymbol{s}'|$.

With straightforward Fourier transform calculations, this approximate form of RTE can be solved analytically. The intensity in the slab at the location $(\boldsymbol{\eta}, \tau)$ in the direction $\boldsymbol{s}$ is [3]

$$I(\boldsymbol{\eta}, \tau, \boldsymbol{s}) = \frac{\mathrm{e}^{-\tau}}{16\pi^4} \iint_{\mathbb{R}^2} \iint_{\mathbb{R}^2} I(\boldsymbol{\kappa}, 0, \boldsymbol{q}) \mathrm{e}^{-\mathrm{i}(\boldsymbol{\eta} - \boldsymbol{s}\tau)\cdot\boldsymbol{\kappa} - \mathrm{i}\boldsymbol{q}\cdot\boldsymbol{s}} \cdot \exp\left\{ \int_0^{\tau} p(\boldsymbol{q} - \boldsymbol{\kappa}\tau') \, \mathrm{d}\tau' \right\} \mathrm{d}\boldsymbol{\kappa} \, \mathrm{d}\boldsymbol{q} \quad (4.1)$$

where $I(\boldsymbol{\kappa}, 0, \boldsymbol{q})$ denotes the Fourier transformed intensity distribution at $\tau = 0$. The exponential contains the Fourier transformed phase function $p(\boldsymbol{q})$, which models the multiple scattering effects.

We ignore intensity contributions to the excitation of the fluorescing dye from all directions except for a cone in the forward direction, $\boldsymbol{s} = \mathbf{0}$, of opening dimension $s_{\max}$. The average contribution in a cone centered in the forward direction is

$$I(\boldsymbol{\eta}, \tau, s_{\max}) = \frac{1}{\pi s_{\max}^2} \iint\limits_{|\boldsymbol{s}| \leq s_{\max}} I(\boldsymbol{\eta}, \tau, \boldsymbol{s}) \, \mathrm{d}\boldsymbol{s}$$

This average has only meaning if $s_{\max}$ is small compared to the beam width of the phase function $p(\boldsymbol{s})$. Finally, as the measurements are performed perpendicular to the laser sheet, the integral of the intensity in the η_y-direction in (4.1) is an accurate model of the intensity recorded, *i.e.*,

$$\langle I(\eta_x, \tau, s_{\max}) \rangle = \int_{-\infty}^{\infty} I(\boldsymbol{\eta}, \tau, s_{\max}) \, \mathrm{d}\eta_y$$

The final expression becomes [3]

$$\begin{aligned} &\langle I(\eta_x, \tau, s_{\max}) \rangle \\ &= \frac{\mathrm{e}^{-\tau}}{4\pi^3} \iint\limits_{\mathbb{R}^2} \int_{-\infty}^{\infty} I(\kappa_x \hat{\boldsymbol{x}}, 0, \boldsymbol{q}) \frac{J_1\left(s_{\max}\sqrt{(q_x - \tau\kappa_x)^2 + q_y^2}\right)}{s_{\max}\sqrt{(q_x - \tau\kappa_x)^2 + q_y^2}} \\ &\quad \exp\left\{-\mathrm{i}\eta_x\kappa_x + \int_0^{\tau} p(\boldsymbol{q} - \kappa_x \hat{\boldsymbol{x}}\tau') \, \mathrm{d}\tau'\right\} \mathrm{d}\kappa_x \, \mathrm{d}\boldsymbol{q} \end{aligned} \quad (4.2)$$

We specialize the incident intensity at $\tau = 0$ and the phase function to a Gaussian form.

$$I(\boldsymbol{\eta}, 0, \boldsymbol{s}) = I_0 \sqrt{\frac{8}{\pi^3}} \frac{\nu}{w\sigma_x\sigma_y} \mathrm{e}^{-2\eta_y^2/w^2 - 2s_x^2/\sigma_x^2 - 2s_y^2/\sigma_y^2} \\ (1 + A\cos(\Theta\eta_x + \delta))$$

and

$$p(\boldsymbol{s}) = \frac{2\alpha}{\pi\beta^2} \mathrm{e}^{-2s^2/\beta^2}$$

The intensity has a beam size $2w$, and $\Theta = 2\pi\nu$, where ν denotes the spatial frequency in the $\hat{\boldsymbol{x}}$ direction. The intensity contains two spread parameters, σ_x and σ_y, which models the divergence of the light intensity. The constant I_0 is the total incident power flux per period in the x direction. β is a measure of the width of the phase function in the forward direction, and α is the single particle albedo. The average intensity in the forward cone is (details of the derivation are found in [3])

$$\begin{aligned} \langle I(\eta_x, \tau, s_{\max}) \rangle = \frac{\nu I_0}{2\pi^2} \mathrm{e}^{-\tau} \iint\limits_{\mathbb{R}^2} \mathrm{e}^{-q_x^2\sigma_x^2/8 - q_y^2\sigma_y^2/8} \\ \left(\frac{J_1\left(s_{\max}\sqrt{q_x^2 + q_y^2}\right)}{s_{\max}\sqrt{q_x^2 + q_y^2}} \exp\left\{\alpha\tau \mathrm{e}^{-(q_x^2+q_y^2)\beta^2/8}\right\} \right. \\ + A\cos(\Theta\eta_x + \delta) \frac{J_1\left(s_{\max}\sqrt{(q_x - \tau\Theta)^2 + q_y^2}\right)}{s_{\max}\sqrt{(q_x - \tau\Theta)^2 + q_y^2}} \\ \left. \exp\left\{\alpha \mathrm{e}^{-q_y^2\beta^2/8} \int_0^{\tau} \mathrm{e}^{-(q_x - \tau'\Theta)^2\beta^2/8} \, \mathrm{d}\tau'\right\} \right) \mathrm{d}\boldsymbol{q} \end{aligned}$$

5 Results

Comparing simulations and experiments requires knowledge of β, $s_{\max}$, σ_x, and σ_y, which are difficult to assess experimentally with adequate accuracy. Ten different simulations were therefore performed, each having a different set of input parameters, permitting us to find the settings that best agreed with our SLIPI results. Our computations verify that the observed reduced extinction of light intensity couples to an increased forward-scattering for large scatterers as was suggested by Kristensson *et al.* [6]. The influence of all these factors on the extinction of light can be seen in Figure 4.

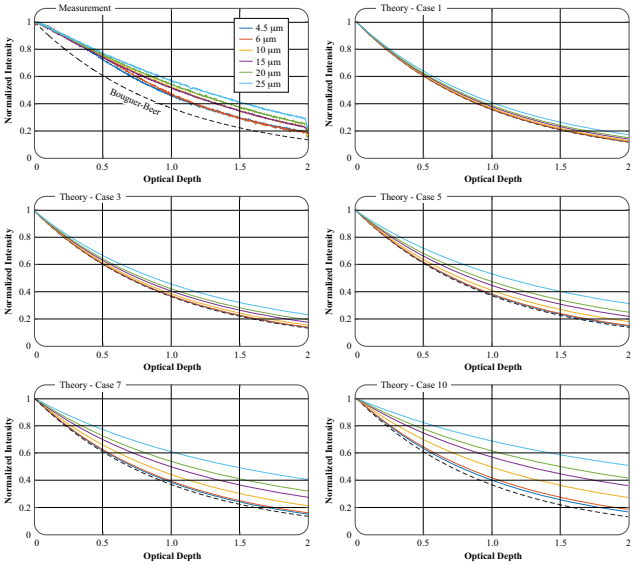

Figure 4: Results from experiments and five of the simulations, showing the local light intensity as a function of optical depth.

From the results shown in Figure 4, it becomes clear that forward-scattering (*i.e.*, the β term) is not solely responsible for the observed deviations from the Bouguer-Beer law. Experimental factors, such as the divergence of the laser sheet, are also important and affect the outcome of a measurement. Figure 5 quantifies the observed deviation from the Bouguer-Beer law for the measurement data as well as for simulation case 5.

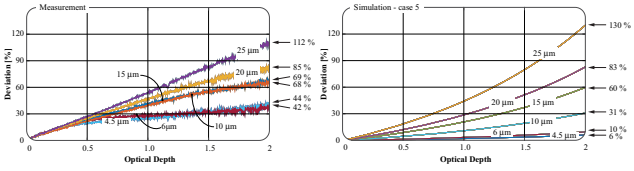

Figure 5: Deviations (in percentage) between the Bouguer-Beer law and the attenuation predicted by our model.

To investigate the influence of the spatial frequency ν on the extinction coefficient, seven SLIPI measurements (Figure 6) were performed. Figure 6 shows normalized attenuation curves of the SLIPI results for the different spatial

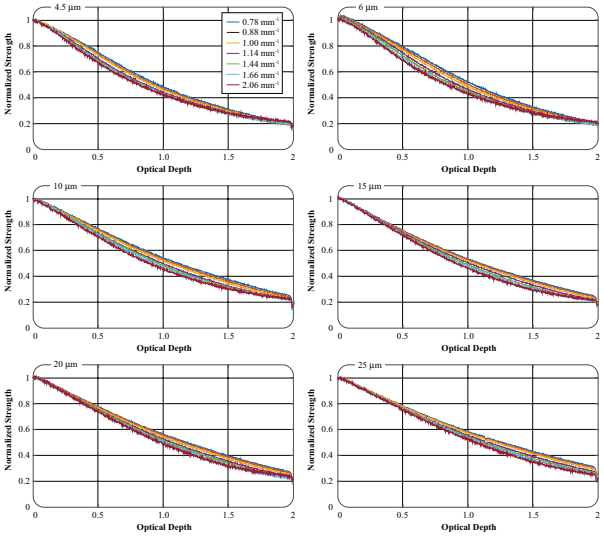

Figure 6: Results from SLIPI experiments performed with seven different spatial frequencies.

frequencies and for all particle sizes. For 25 μm, the effect is strongest, and the acquired data reveals that, as the spatial frequency increases, the light appears to be attenuated more rapidly with distance. Figure 7 shows that the evaluated extinction coefficient gradually increases for larger particles as the modulation frequency becomes finer, while for smaller particles it stagnates at ≈ 0.043 mm^{-1}, never fully reaching the expected value of 0.045 mm^{-1} as predicted by the Bouguer-Beer law. If these extinction coefficients are plotted as a function of $\nu/2\pi r$, where r is the radius of the particles in mm, an interesting trend appears, see Figure 8. The data shows that regardless of the particle size, a SLIPI measurement performed with a relatively low modulation frequency gives results that deviates from the Bouguer-Beer law or, equivalently, the sample appears less turbid.

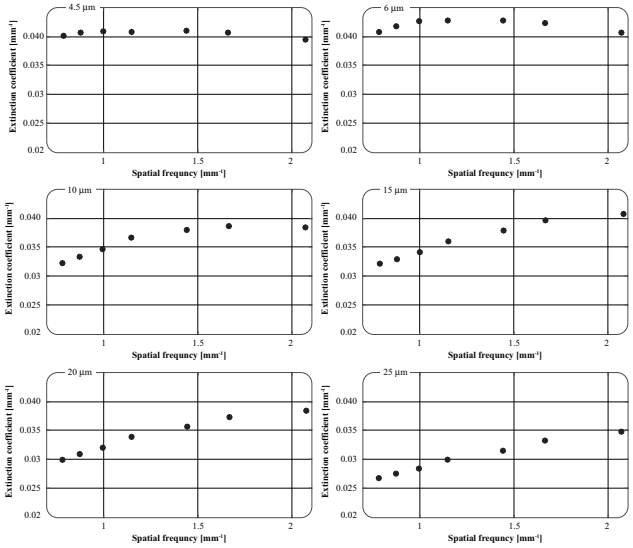

Figure 7: The evaluated extinction coefficient for the measurement cases presented in Figure 6.

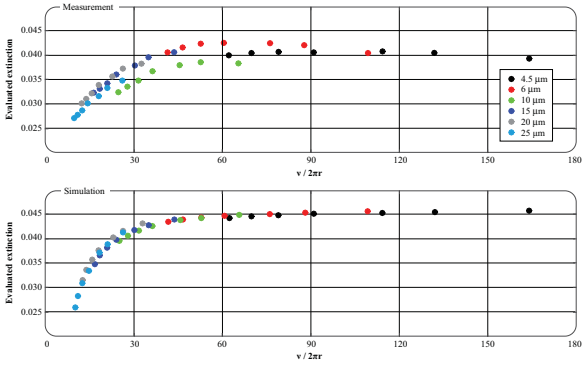

Figure 8: The extinction coefficient data in Figure 7, plotted as a function of $\nu/2\pi r$.

6 Discussion and conclusions

The experiments and the theoretical predictions are in good agreement, both clearly showing how the current conception of light extinction by the Bouguer-Beer law is not completely accurate in these turbid environments. For example, the model shows that the measurable opacity of a homogeneous sample with particles of 25 μm in diameter with the current optical arrangement is reduced by roughly 130% at an expected optical depth of 2. Moreover, our study demonstrates how the deviation from this law can be quantified, potentially opening up for a new strategy to determine particle size.

References

[1] E. Kristensson, E. Berrocal, and M. Aldén, "Two-pulse structured illumination imaging," *Optics letters*, vol. 39, no. 9, pp. 2584–2587, 2014.

[2] R. Neil, M.A.A. Juskaitis and T. Wilson, "Method of obtaining optical sectioning by using structured light in a conventional microscope," *Optics Letters*, vol. 22, no. 24, pp. 1905–1907, 1997.

[3] E. Kristensson and G. Kristensson, "Physical explanation of the SLIPI technique by the large scatter approximation of the RTE," *J. Quant. Spectrosc. Radiat. Transfer*, vol. 189, pp. 112–125, 2017.

[4] A. Ishimaru, *Wave Propagation and Scattering in Random Media*. New York: IEEE Press, 1997.

[5] X. Ma, J. Q. Lu, R. S. Brock, K. M. Jacobs, P. Yang, and X.-H. Hu, "Determination of complex refractive index of polystyrene microspheres from 370 to 1610 nm," *Physics in medicine and biology*, vol. 48, no. 24, p. 4165, 2003.

[6] E. Kristensson, L. Araneo, E. Berrocal, J. Manin, M. Richter, M. Aldén, and M. Linne, "Analysis of multiple scattering suppression using structured laser illumination planar imaging in scattering and fluorescing media," *Optics Express*, vol. 19, no. 14, pp. 13 647–13 663, 2011.